Published in final edited form as:
Am J Ophthalmol. 2011 November ; 152(5): 807–814.e1. doi:10.1016/j.ajo.2011.04.027.

Feasibility of a Method for Enface Imaging of Photoreceptor Cell Integrity

Justin Wanek, **Ruth Zelkha**, **Jennifer I. Lim**, and **Mahnaz Shahidi**
Department of Ophthalmology & Visual Sciences, University of Illinois at Chicago

Abstract

Purpose—To report a method for enface imaging of the photoreceptor inner and outer segment junction by spectral domain optical coherence tomography (SDOCT) and describe findings in normal subjects and patients with various retinal diseases.

Design—Observational case series study.

Materials and Methods—SDOCT images were acquired in six normal subjects (44 ± 11 years) and five subjects with retinal diseases (66 ± 22 years). A customized high density SDOCT volume scan was acquired on the retina. SDOCT B-scan images were automatically segmented to extract intensity data along the inner and outer segment junction. Data obtained from the raster B-scans were combined to generate an inner and outer segment enface image in a 4.4 mm × 4.4 mm retinal area, centered on the fovea. The foveal to parafoveal mean intensity ratio was measured and repeatability was determined. An infrared (IR) scanning laser ophthalmoscope (SLO) image was acquired and cropped to provide a field of view similar to the inner and outer segment enface image.

Results—Inner and outer segment enface images generated in normal subjects provided clear visualization of the retinal vasculature, matching the vascular network observed in the IR SLO image. In normal subjects, the foveal to parafoveal mean intensity ratio was 0.88 ± 0.06 and repeatability of measurements was on average 7%. In macular hole, a dark circular region was observed in the inner and outer segment enface image, indicative of photoreceptor cell loss. In age-related macular degeneration, the enface image displayed non-uniform texture corresponding to topographic variations in the inner and outer segment junction. In central serous retinopathy, areas of lower intensity were visible on the enface image, corresponding to regions of prior neurosensory elevation. In cystoid macular edema, reduced intensity was present in the inner and outer segment enface image in areas with increased retinal thickness. In diabetic retinopathy, the inner and outer segment enface image displayed regions of reduced intensity due to edema and/or laser scars.

Conclusion—Detection of intensity abnormalities in the inner and outer segment enface image is useful for monitoring the integrity of photoreceptor cells in the course of disease progression and therapeutic intervention.

Corresponding Author: Mahnaz Shahidi, Ph.D., Department of Ophthalmology and Visual Sciences, University of Illinois at Chicago, 1855 West Taylor Street, Chicago IL 60612, Tel: 312-413-7364, Fax: 312-413-7366, mahnshah@uic.edu.

Introduction

The availability of spectral domain optical coherence tomography (SDOCT) has improved visualization and delineation of retinal substructures. In particular, the junction of the inner and outer segments of the photoreceptors has been visualized on SDOCT B-scans.[1–3] Recent studies have shown an association between visual acuity and continuity (integrity) of the inner and outer segment junction in patients with retinitis pigmentosa,[4–6] Stargardt's disease,[7] retinal vein occlusion,[8, 9] age-related macular degeneration (AMD),[10] and resolved central serous chorioretinopathy.[11, 12] Additionally, both photoreceptor outer segment length and continuity of the inner and outer segment junction have been shown to affect visual function of patients with diabetic macular edema.[13, 14] To our knowledge, few methods have evaluated the integrity of the inner and outer segment junction in an enface manner.[15, 16] In this study, we report a new automated image reconstruction method based on SDOCT imaging to generate enface images of the inner and outer segment junction and describe findings in normal subjects and patients with various retinal diseases.

Materials and Methods

Subjects

Six visually normal subjects (3 females and 3 males) and five subjects with retinal diseases (2 females and 3 males) participated in the study. Data was obtained in one eye of normal subjects and in one or both eyes of subjects with retinal pathologies. Ages of normal subjects ranged from 30 to 58 years, with a mean age of 44 ± 11 years (mean ± standard deviation), while ages of subjects with retinal diseases ranged from 35 to 92 years, with a mean age of 66 ± 22 years.

Image Acquisition

SDOCT images were acquired using a commercially available instrument (Spectralis, Heidelberg, Germany). A high density SDOCT volume scan centered on the macular area was acquired. The OCT volume scan consisted of 145 raster B-scans images, each 768 pixels in length (5.7 μm/pixel) and separated by 31 μm, thus covering an area of 4.4 mm × 4.4 mm on the retina. The number of pixels in depth (vertical dimension of the B-scan image) varied among images due to the instrument's eye tracking capability, but the depth resolution was constant (3.9 μm/pixel). The instrument's eye tracker allowed multiple B-scans to be averaged at a single location. The time for acquiring the OCT volume scan varied depending on fixation stability of the subject, but was typically less than 20 seconds. An infrared (IR) scanning laser ophthalmoscope (SLO) image was acquired with the same instrument to document the area of imaging. To provide a field of view similar to the inner and outer segment enface image, the IR SLO image was cropped and intensity levels were adjusted, thereby improving visualization of retinal features.

Image Segmentation

The inner and outer segment junction was automatically segmented from each B-scan image using software developed in MATLAB (The Mathworks Inc, Natick, Massachusetts, USA). The inner and outer segment junction is typically characterized in OCT images as a thin reflective layer, posterior to the weak reflecting (dark) outer nuclear layer (ONL) and anterior to the strong reflecting (bright) retinal pigment epithelium (RPE) complex. In general, the segmentation algorithm identified the inner and outer segment junction by searching for a local intensity maximum between the ONL and RPE. First, each B-scan image was divided into vertical sections of equal width. The width of the vertical section was empirically assigned to 16 pixels, thereby identifying the inner and outer segment junction at 91 μm intervals along the horizontal dimension of the SDOCT B-scan. For each

section, a mean intensity profile was computed by horizontal averaging of pixel intensities and a low-pass filter was used to further smooth the profile, as shown in Figure 1. From the smoothed profile, the locations of the 2 largest peaks were obtained, corresponding to the RPE and inner limiting membrane. Subsequently, the location of the local minimum between the two peaks was found, corresponding to the ONL. Finally, from the mean intensity profile, the location of the largest peak between the local minimum and the posterior peak (RPE) of the smoothed profile was obtained, corresponding to the inner and outer segment junction. If no peak was found in the final step or the inner and outer segment junction was more than 80 μm anterior to the RPE, no inner and outer segment junction location was stored for the particular section. These steps were repeated for each vertical section and a continuous line was drawn by interpolation between inner and outer segment junction locations.

Image Reconstruction and Analysis

An inner and outer segment enface image was generated by extracting the intensity data along the inner and outer segment junction in each B-scan image and storing the data in consecutive rows of the enface image. The inner and outer segment junction thickness varied between 3 to 5 pixels, based on inspection of B-scans in normal subjects. Therefore, the intensity data of the line defining the inner and outer segment junction with 5 pixel (20 μm) width was extracted using bilinear interpolation and the data was stored as 5 rows along the inner and outer segment enface image. This procedure was repeated for each B-scan image to generate an inner and outer segment enface image. The inner and outer segment enface image was then resampled to adjust the vertical dimension of the image, yielding a square image of 768 × 768 pixels. Lastly, a smoothing filter that vertically averaged every 5 pixels was applied to the inner and outer segment enface image, thereby diminishing horizontal lines that appeared due to reflectance variations of the inner and outer segment junction among B-scan images acquired from the same subject.

Inner and outer segment enface images were analyzed by calculating the mean of intensity values in two retinal circular areas with dimensions defined according to the Early Treatment Diabetic Retinopathy Study.[17] The foveal area encompassed a circular region 1.2 mm in diameter centered on the fovea and the parafoveal area encompassed a concentric ring with inner and outer diameters of 1.2 and 3.1 mm, respectively. The ratio of the mean intensity of foveal to parafoveal areas was determined. As compared to mean intensity values, the ratio is a more reliable parameter since it accounts for variations between visits and among subjects due to optical factors. Repeatability was assessed by the percent difference of foveal to parafoveal mean intensity ratio measurements obtained from two repeated images in five normal subjects.

Results

Normal Subjects

The segmentation of the inner and outer segment junction for 3 typical B-scans, acquired at the fovea, superior and inferior to the fovea in the right eye of a normal 30 year old male subject is displayed in Figure 2. Visual acuity in the right eye was 20/20. The algorithm correctly identified the inner and outer segment junction in each B-scan, as shown by the continuous white line overlaid on the B-scan images. The reconstructed inner and outer segment enface image displayed retinal vasculature due to shadowing of the vessels on the inner and outer segment junction, matching the vascular network observed in IR SLO image. The high intensity spot present in the center of the IR image is an artifact associated with the instrument and is unrelated to the retina.

The inner and outer segment enface image from the right eye of a normal 31 year old male subject with 20/20 visual acuity is displayed in Figure 3. A focal dark spot was detected on the inner and outer segment enface image at a location superonasal to the fovea. The corresponding B-scan revealed a small discontinuity in the inner and outer segment junction at the location of the dark spot. Among normal subjects, the foveal to parafoveal mean intensity ratio ranged between 0.79 and 0.94 and was on average 0.88 ± 0.06 (mean ± SD; N = 6). Repeatability of the intensity ratio was on average 7% (N = 5).

Case 1: Age-related Macular Degeneration and Macular Hole—A 68 year old female with a history of neovascular age-related macular degeneration (AMD) in the left eye, four months following pars plana vitrectomy for a macular hole in the left eye, underwent SDOCT imaging. The macular hole was observed to be closed on clinical examination. Visual acuity post-operatively in the left eye was 20/60 (pinhole without improvement). Examples of applying the inner and outer segment segmentation algorithm to B-scans are shown in Figure 4. For locations with an absent inner and outer segment junction, the position was estimated by interpolating between the nearest locations where the inner and outer segment junctions were found, as described in the methods section. The macular hole was observed in the inner and outer segment enface image as a dark circular region due to the absence of reflectance from the inner and outer segment junction. The foveal to parafoveal mean intensity ratio was 0.58, lower than the range in normal subjects. In addition, the adjacent retinal cysts were also visualized on the enface image.

Case 2: Age-related Macular Degeneration—An 80 year old male with a history of an eccentric neovascular lesion due to AMD was imaged in the left eye. The subject had undergone a combined phacoemulsification with intraocular lens implantation with pars plana vitrectomy for a mature cataract and a dense vitreous hemorrhage caused by an eccentric disciform scar. Drusen and RPE mottling in the central macular area were present postoperatively on clinical examination. Visual acuity in the left eye was 20/25. Examples of B-scans, the inner and outer segment enface image, and the IR SLO image are shown in Figure 5. Small and localized elevations of the inner and outer segment junction due to the underlying drusen and RPE changes were visible in the B-scans. Topographic variations in the inner and outer segment junction were displayed in the inner and outer segment enface image as regions with non-uniform texture, particularly inferior to the fovea where areas with slightly higher intensity were observed. The visible intensity variation along rows of the image and the mildly discontinuous vascular network were attributed to limited fixation stability of the subject, resulting in variations in the reflectance from the inner and outer segment junction among B-scans.

Case 3: Central Serous Retinopathy—A 35 year old male with a three year history of central serous retinopathy (CSR) underwent SDOCT imaging. The subject had RPE mottling and no current activity of the CSR (no pigment epithelial detachment or subretinal fluid) on clinical examination. Visual acuity in the left eye was 20/20. Examples of B-scans, the inner and outer segment enface image, and the IR SLO image are shown in Figure 6. The inner and outer segment enface image displayed some regions of lower intensity due to decreased reflectance from the inner and outer segment junction, mostly inferior and nasal to the fovea, corresponding to areas of prior neurosensory elevation associated with the site of CSR. These regions were well delineated on the inner and outer segment enface image.

Case 4: Cystoid Macular Edema—A 56 year old male with a history of retinal detachment surgery and pars plana vitrectomy surgery for a macular hole (slightly eccentric) underwent SDOCT imaging. Visual acuity in the left eye was 20/25. Examples of B-scans, the inner and outer segment enface image, and the IR SLO image are shown in Figure 7. The

subject had cystoid macular edema and subfoveal fluid, as seen on the foveal B-scan. The inner and outer segment junction was not visible under the edema, but visualized in parafoveal areas that did not have considerable thickening. The inner and outer segment enface image displayed a large central region of reduced or no intensity, corresponding to the area of macular edema. The foveal to parafoveal mean intensity ratio was 0.16, considerably lower than the average in normal subjects, indicative of reduced visibility of the inner and outer segment junction in the foveal area.

Case 5: Diabetic Retinopathy—A 92 year old female was diagnosed with diabetic retinopathy (DR) and clinically significant diabetic macular edema in the left eye. The subject had a prior history of cataract surgery with intraocular lens implantation in both eyes and focal laser treatment in the left eye, followed by intravitreal injections of bevacizumab. Visual acuity in the left eye with her current eyeglasses was 20/200 (pinhole 20/80). Examples of B-scans, the inner and outer segment enface image, and the IR SLO image are shown in Figure 8. The B-scan at the fovea displayed macular edema with large cysts in the inner nuclear layer and some loss of reflectance from the underlying inner and outer segment junction. Focal areas of reduced reflectance of the inner and outer segment junction were also observed in the B-scan superior to the fovea. The inner and outer segment enface image revealed several regions of localized reduced intensity due to the presence of edema and/or focal laser scars.

Discussion

The brightness of the photoreceptor cell inner and outer segment junction as visualized by cross sectional SDOCT imaging has been shown to be related to visual function in several retinal diseases.[18–21] Additionally, the integrity of the photoreceptor cell inner and outer segment junction may provide useful information for visual function outcome following treatment.[16, 22, 23] Recently, SDOCT imaging has been utilized for three dimensional imaging of retinal pathologies.[15, 16, 24–26] In the current study, an image segmentation and reconstruction method for generating an enface image of the photoreceptor cell inner and outer segment junction is reported. In subjects with retinal diseases, focal regions with no reflectance or reduced and/or non-uniform intensity levels were observed on inner and outer segment enface images, clearly delineating areas of pathologies.

The inner and outer segment enface image is reconstructed from a single interface within the retinal tissue from high depth resolution SDOCT images, therefore it has high contrast and offers an accurate delineation of the spatial extent of retinal pathologies. Additionally, inner and outer segment enface images are superior as compared to individual SDOCT B-scan images, allowing distinction of blood vessel shadowing (due to absorption of light by hemoglobin) from true discontinuity in the inner and outer segment junction. Furthermore, since inner and outer segment enface imaging targets visualization of structures at a specific retinal depth, it is useful for assessment of the photoreceptor cell integrity in various retinal diseases and conditions.

In the current study, the foveal to parafoveal mean intensity ratio calculated from inner and outer segment enface images in normal subjects was comparable to previously published measurements from SDOCT B-scan images.[16] In addition, the visible vascular pattern on the inner and outer segment enface images in normal subjects was consistent with findings on SDOCT enface images in a previous study.[15, 27] In the case of AMD and macular hole, the inner and outer segment enface image displayed a dark circular region at the fovea, providing distinct visualization of the complete disruption of photoreceptor integrity, similar to enface images generated in patients with macular holes in a previous study.[16] In AMD, the inner and outer segment enface image showed non-uniform texture and focal areas with

higher intensities, corresponding to topographic variations in the photoreceptor inner and outer segment junction. This non-uniformity is consistent with the reported intensity variations in AMD enface images due to drusen.[15, 27] In CSR, on the inner and outer segment enface image, regions with reduced intensities were visible, corresponding to areas of prior neurosensory elevation. In cystoid macular edema, the inner and outer segment image showed reduced intensities in areas with retinal thickening, as compared to parafoveal areas without considerable thickening. In DR, the inner and outer segment enface image displayed localized regions with reduced intensities, attributed to the presence of edema and/or laser scars.

As with all imaging technologies, the ability to identify localized retinal pathologies depends on image quality. Despite the eye tracking capabilities of the instrument, a lack of adequate fixation stability in some subjects may cause intensity variations among B-scans, corresponding to non-uniformity along rows in the inner and outer segment enface image and discontinuity in the visualized vascular pattern. Additionally, the presence of macular edema may present a reduced or complete lack of reflectance from the inner and outer segment junction. In these cases, the cause of intensity reduction of the inner and outer segment enface image may be pathological due to disruption of the photoreceptor integrity and/or optical due to absorption of light by the intraretinal fluid. Future studies are needed to determine the contributions of these factors on the reversibility of photoreceptor inner and outer segment junction reflectance and/or visual loss following treatment of macular edema. With further development and application to a wide range of retinal diseases, this method has the potential to aid retina specialists in clinical practice. Specifically, changes in the inner and outer segment junction could be better evaluated and monitored using an enface map rather than detecting discontinuities in individual B-scan images. Overall, the application of this method for mapping disruptions in the photoreceptor cell inner and outer segment junction is of potential value in assessment of visual outcome following therapeutic intervention.

Acknowledgments

a. *Funding / Support (including none):* NIH grants EY14275 (MS) and EY01792 (UIC), Bethesda, Maryland; Department of Veterans Affairs, Washington, DC, a senior scientific investigator award (MS) and an unrestricted departmental grant from Research to Prevent Blindness, Inc., New York, New York, and the Gerhard Cless Retina Research Fund.

b. Financial Disclosures (including none): None

c. *Contributions to Authors in each of these areas:* Design of the study (MS); conduct of the study (JW,MS); collection, management, analysis, and interpretation of the data (RZ, JL, JW, MS); preparation, review, or approval of the manuscript (JW, JL, MS).

d. *Statement about Conformity with Author Information:* The research study was approved by an institutional review board of the University of Illinois at Chicago. Informed consent according to the tenets of Helsinki for participation in the research and HIPAA compliance were obtained.

e. Other Acknowledgments: None.

References

1. Drexler W, Sattmann H, Hermann B, et al. Enhanced visualization of macular pathology with the use of ultrahigh-resolution optical coherence tomography. Arch Ophthalmol. 2003; 121(5):695–706. [PubMed: 12742848]
2. Gloesmann M, Hermann B, Schubert C, Sattmann H, Ahnelt PK, Drexler W. Histologic correlation of pig retina radial stratification with ultrahigh-resolution optical coherence tomography. Invest Ophthalmol Vis Sci. 2003; 44(4):1696–1703. [PubMed: 12657611]

3. Costa RA, Calucci D, Skaf M, et al. Optical coherence tomography 3: Automatic delineation of the outer neural retinal boundary and its influence on retinal thickness measurements. Invest Ophthalmol Vis Sci. 2004; 45(7):2399–2406. [PubMed: 15223823]
4. Sandberg MA, Brockhurst RJ, Gaudio AR, Berson EL. The association between visual acuity and central retinal thickness in retinitis pigmentosa. Invest Ophthalmol Vis Sci. 2005; 46(9):3349–3354. [PubMed: 16123439]
5. Rangaswamy NV, Patel HM, Locke KG, Hood DC, Birch DG. A comparison of visual field sensitivity to photoreceptor thickness in retinitis pigmentosa. Invest Ophthalmol Vis Sci. 2010; 51(8):4213–4219. [PubMed: 20220048]
6. Wakabayashi T, Sawa M, Gomi F, Tsujikawa M. Correlation of fundus autofluorescence with photoreceptor morphology and functional changes in eyes with retinitis pigmentosa. Acta Ophthalmol. 2010; 88(5):e177–e183. [PubMed: 20491687]
7. Ergun E, Hermann B, Wirtitsch M, et al. Assessment of central visual function in Stargardt's disease/fundus flavimaculatus with ultrahigh-resolution optical coherence tomography. Invest Ophthalmol Vis Sci. 2005; 46(1):310–316. [PubMed: 15623790]
8. Ota M, Tsujikawa A, Murakami T, et al. Foveal photoreceptor layer in eyes with persistent cystoid macular edema associated with branch retinal vein occlusion. Am J Ophthalmol. 2008; 145(2):273–280. [PubMed: 18045566]
9. Shin HJ, Chung H, Kim HC. Association between integrity of foveal photoreceptor layer and visual outcome in retinal vein occlusion. Acta Ophthalmol. 2011; 89(1):e35–e40. [PubMed: 21155986]
10. Hayashi H, Yamashiro K, Tsujikawa A, Ota M, Otani A, Yoshimura N. Association between foveal photoreceptor integrity and visual outcome in neovascular age-related macular degeneration. Am J Ophthalmol. 2009; 148(1):83–89. e81. [PubMed: 19327745]
11. Eandi CM, Chung JE, Cardillo-Piccolino F, Spaide RF. Optical coherence tomography in unilateral resolved central serous chorioretinopathy. Retina. 2005; 25(4):417–421. [PubMed: 15933586]
12. Piccolino FC, de la Longrais RR, Ravera G, et al. The foveal photoreceptor layer and visual acuity loss in central serous chorioretinopathy. Am J Ophthalmol. 2005; 139(1):87–99. [PubMed: 15652832]
13. Forooghian F, Stetson PF, Meyer SA, et al. Relationship between photoreceptor outer segment length and visual acuity in diabetic macular edema. Retina. 2010; 30(1):63–70. [PubMed: 19952996]
14. Maheshwary AS, Oster SF, Yuson RM, Cheng L, Mojana F, Freeman WR. The association between percent disruption of the photoreceptor inner segment-outer segment junction and visual acuity in diabetic macular edema. Am J Ophthalmol. 2010; 150(1):63–67. e61. [PubMed: 20451897]
15. Wojtkowski M, Sikorski BL, Gorczynska I, et al. Comparison of reflectivity maps and outer retinal topography in retinal disease by 3-D Fourier domain optical coherence tomography. Opt Express. 2009; 17(5):4189–4207. [PubMed: 19259255]
16. Oh J, Smiddy WE, Flynn HW Jr, Gregori G, Lujan B. Photoreceptor inner/outer segment defect imaging by spectral domain OCT and visual prognosis after macular hole surgery. Invest Ophthalmol Vis Sci. 2010; 51(3):1651–1658. [PubMed: 19850825]
17. Early Treatment Diabetic Retinopathy Study design and baseline patient characteristics. ETDRS report number 7. Ophthalmology. 1991; 98 5 Suppl:741–756. [PubMed: 2062510]
18. Inoue M, Watanabe Y, Arakawa A, Sato S, Kobayashi S, Kadonosono K. Spectral-domain optical coherence tomography images of inner/outer segment junctions and macular hole surgery outcomes. Graefes Arch Clin Exp Ophthalmol. 2009; 247(3):325–330. [PubMed: 19018552]
19. Michalewska Z, Michalewski J, Cisiecki S, Adelman R, Nawrocki J. Correlation between foveal structure and visual outcome following macular hole surgery: a spectral optical coherence tomography study. Graefes Arch Clin Exp Ophthalmol. 2008; 246(6):823–830. [PubMed: 18386040]
20. Sayanagi K, Ikuno Y, Soga K, Tano Y. Photoreceptor inner and outer segment defects in myopic foveoschisis. Am J Ophthalmol. 2008; 145(5):902–908. [PubMed: 18342829]

21. Suh MH, Seo JM, Park KH, Yu HG. Associations between macular findings by optical coherence tomography and visual outcomes after epiretinal membrane removal. Am J Ophthalmol. 2009; 147(3):473–480. e473. [PubMed: 19054492]

22. Cunha-Vaz J, Coscas G. Diagnosis of macular edema. Ophthalmologica. 2010; 224 Suppl 1 2–7.

23. Wakabayashi T, Fujiwara M, Sakaguchi H, Kusaka S, Oshima Y. Foveal microstructure and visual acuity in surgically closed macular holes: spectral-domain optical coherence tomographic analysis. Ophthalmology. 2010; 117(9):1815–1824. [PubMed: 20472291]

24. Hangai M, Ojima Y, Gotoh N, et al. Three-dimensional imaging of macular holes with high-speed optical coherence tomography. Ophthalmology. 2007; 114(4):763–773. [PubMed: 17187861]

25. Schmidt-Erfurth U, Leitgeb RA, Michels S, et al. Three-dimensional ultrahigh-resolution optical coherence tomography of macular diseases. Invest Ophthalmol Vis Sci. 2005; 46(9):3393–3402. [PubMed: 16123444]

26. Srinivasan VJ, Wojtkowski M, Witkin AJ, et al. High-definition and 3-dimensional imaging of macular pathologies with high-speed ultrahigh-resolution optical coherence tomography. Ophthalmology. 2006; 113(11) 2054 e2051-2014.

27. Gorczynska I, Srinivasan VJ, Vuong LN, et al. Projection OCT fundus imaging for visualizing outer retinal pathology in non-exudative age-related macular degeneration. Br J Ophthalmol. 2009; 93(5):603–609. [PubMed: 18662918]

Biography

Justin Wanek, M.S. is a research specialist of the Department of Ophthalmology and Visual Sciences at the University of Illinois at Chicago. Mr. Wanek is a graduate of the University of Wisconsin-Madison were he received degrees in engineering mechanics and astronautics and civil and environmental engineering. Mr. Wanek's research interests include development of optical instrumentation for ophthalmic imaging and image processing techniques for quantitative assessment of the retina.

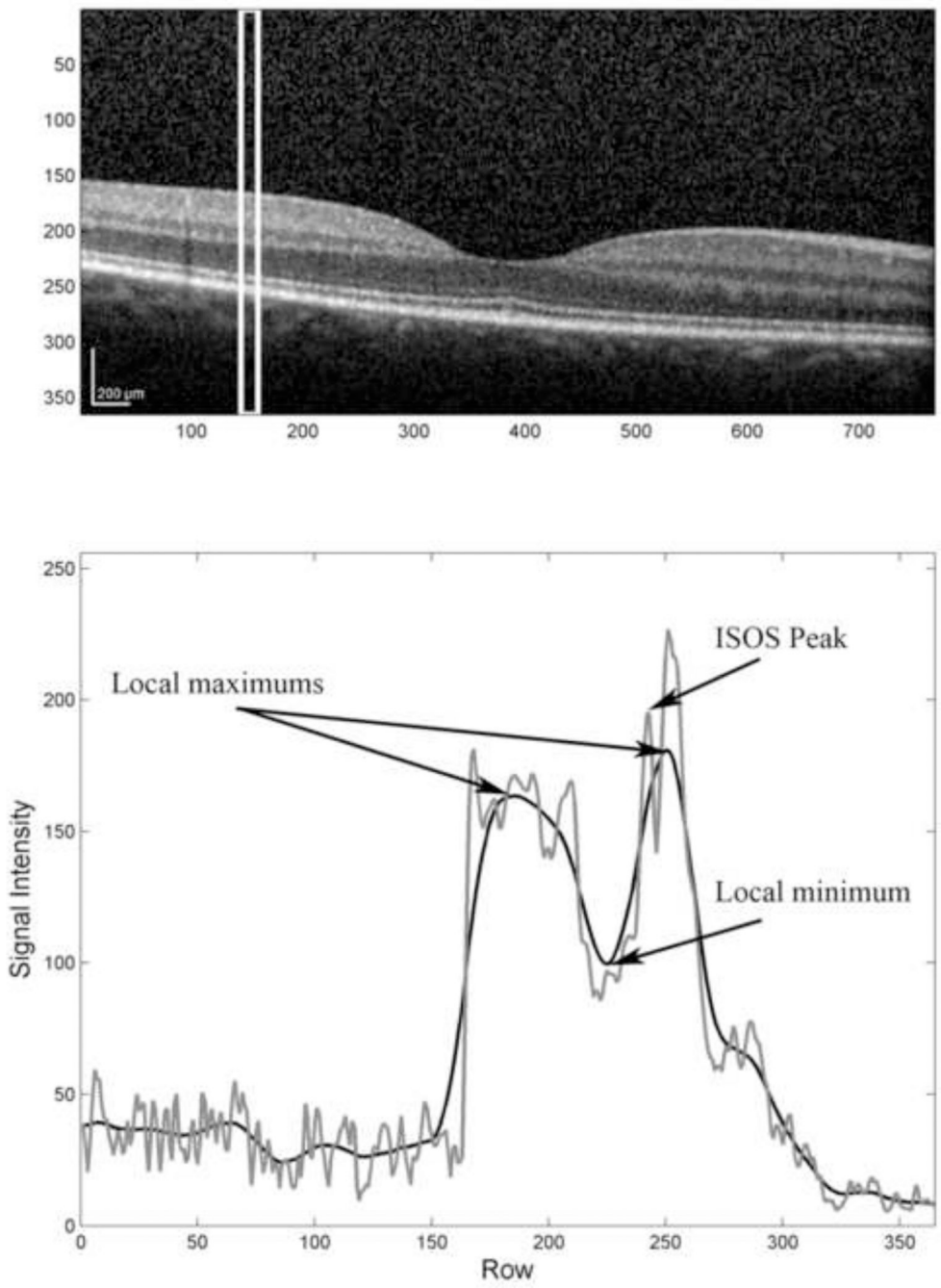

Figure 1.

(Top) An example of a SDOCT B-scan acquired in a normal subject. (Bottom) The mean intensity profile (gray) was derived by horizontal averaging of pixel values within the region of interest shown in (Top). The locations of two maximums and the minimum (indicated with arrows) were determined from the smoothed intensity profile (black). The location of the largest local maximum (indicated with an arrow) of the mean intensity profile (gray) that occurred between the local minimum and the posterior maximum of the smoothed intensity profile coincided with the inner and outer segment junction.

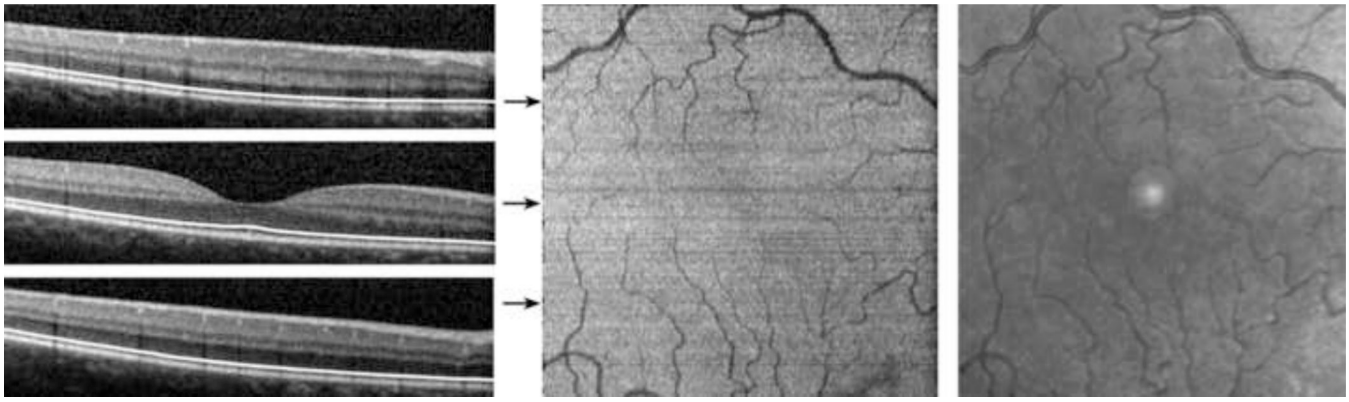

Figure 2.
Normal Subject: (Left) Examples of SDOCT B-scans with the automatically detected inner and outer segment junction shown with white lines. (Center) A reconstructed inner and outer segment enface image of a 4.4 mm × 4.4 mm retinal area centered on the fovea. Location of B-scans shown in (Left) are marked by horizontal arrows. (Right) A cropped infrared SLO image acquired with the SLO/OCT instrument. The high intensity spot present in the center of the IR image is an artifact associated with the instrument and is unrelated to the retina.

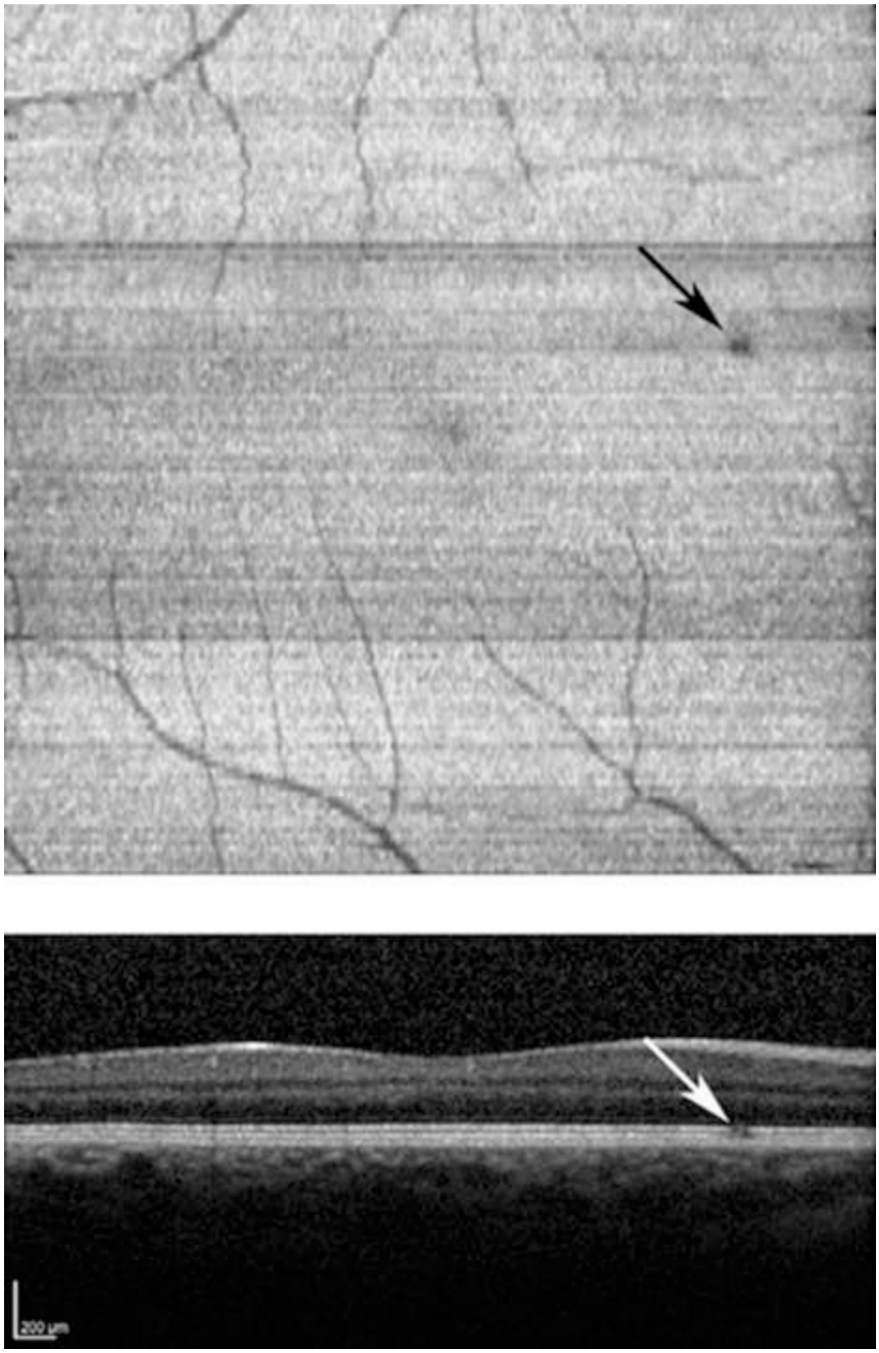

Figure 3.
Normal Subject: (Top) An inner and outer segment enface image from a normal subject, revealing a focal dark region located superonasal to the fovea (black arrow). (Bottom) A SDOCT B-scan traversing the dark region in (Top). A small discontinuity in the inner and outer segment junction is marked with a white arrow.

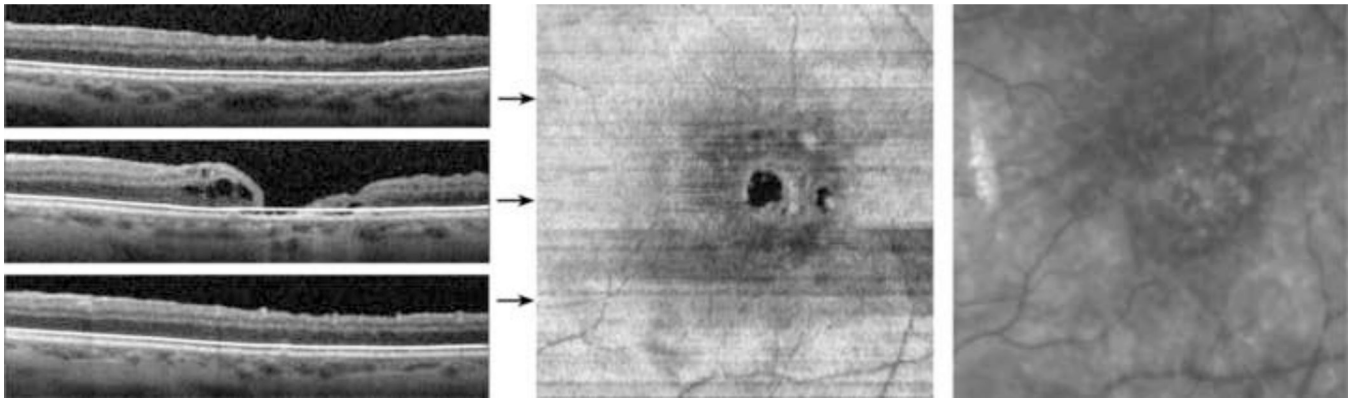

Figure 4.
Age-related Macular Degeneration and Macular Hole: (Left) Examples of SDOCT B-scans with the detected inner and outer segment junction shown with white lines. (Center) The inner and outer segment enface image. Horizontal arrows indicate the location of the B-scans. (Right) A cropped infrared SLO image acquired with the SLO/OCT instrument.

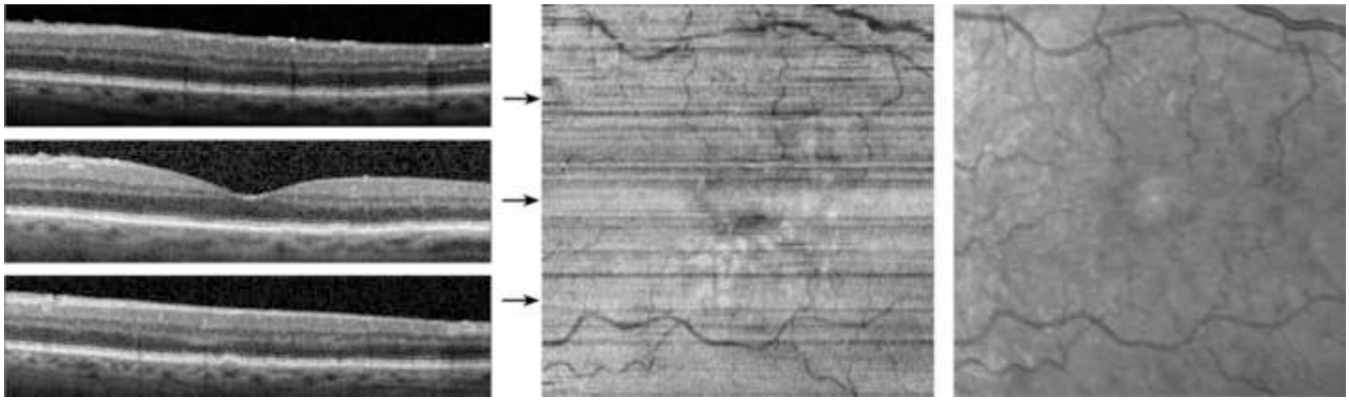

Figure 5.

Age-related Macular Degeneration: (Left) Examples of SDOCT B-scans. (Center) The inner and outer segment enface image. Horizontal arrows indicate the location of the B-scans. (Right) A cropped infrared SLO image acquired with the SLO/OCT instrument.

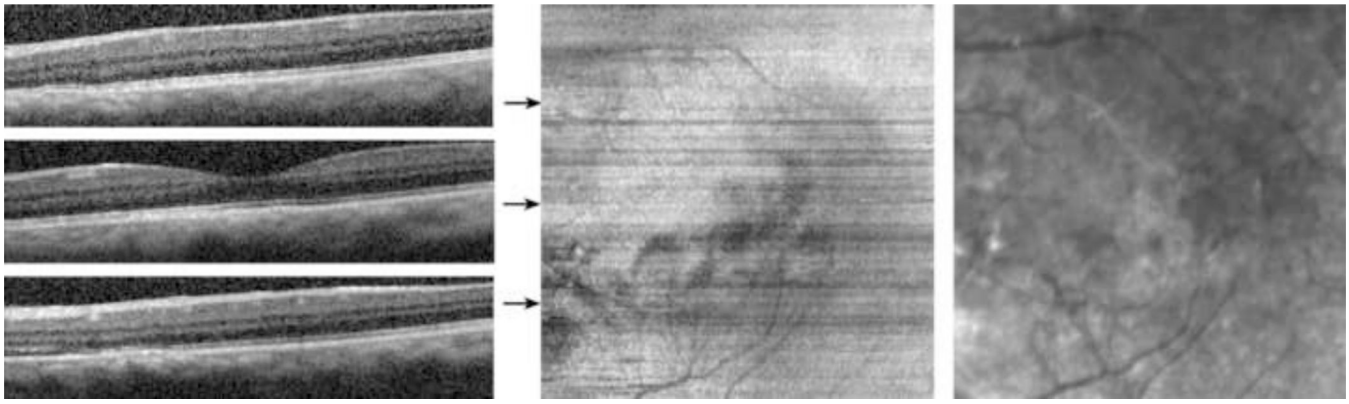

Figure 6.
Central Serous Retinopathy: (Left) Examples of SDOCT B-scans. (Center) The inner and outer segment enface image. Horizontal arrows indicate the location of the B-scans. (Right) A cropped infrared SLO image acquired with the SLO/OCT instrument.

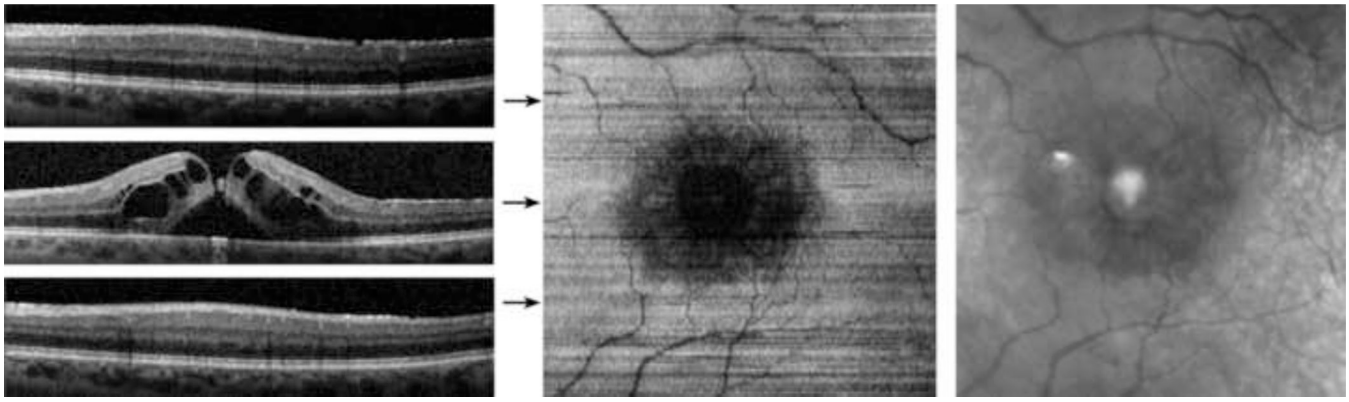

Figure 7.
Cystoid Macular Edema: (Left) Examples of SDOCT B-scans. (Center) The inner and outer segment enface image. Horizontal arrows indicate the location of the B-scans. (Right) A cropped infrared SLO image acquired with the SLO/OCT instrument.

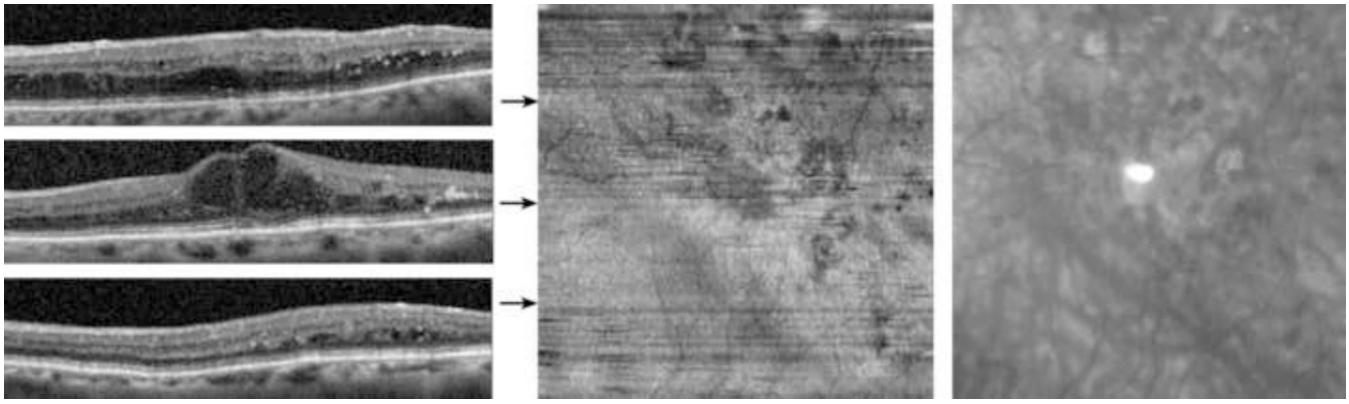

Figure 8.
Diabetic Retinopathy: (Left) Examples of SDOCT B-scans. (Center) The inner and outer segment enface image. Horizontal arrows indicate the location of the B-scans. (Right) A cropped infrared SLO image acquired with the SLO/OCT instrument.